The influence of atmospheric blocking on extreme winter minimum temperatures in North America

Kirien Whan, Francis W. Zwiers, & Jana Sillmann

2016

Original citation:

Whan, K., Zwiers, F. W., & Sillmann, J. (2016). The influence of atmospheric blocking on extreme winter minimum temperatures in North America. *Journal of Climate*, *29*(12), 4361–4381. https://doi.org/10.1175/JCLI-D-15-0493.1

The Influence of Atmospheric Blocking on Extreme Winter Minimum Temperatures in North America

KIRIEN WHAN AND FRANCIS ZWIERS

Pacific Climate Impacts Consortium, University of Victoria, Victoria, British Columbia, Canada

JANA SILLMANN

Center for International Climate and Environmental Research, Oslo, Norway

(Manuscript received 15 July 2015, in final form 18 December 2015)

ABSTRACT

Regional climate models (RCMs) are the primary source of high-resolution climate projections, and it is of crucial importance to evaluate their ability to simulate extreme events under current climate conditions. Many extreme events are influenced by circulation features that occur outside, or on the edges of, RCM domains. Thus, it is of interest to know whether such dynamically controlled aspects of extremes are well represented by RCMs. This study assesses the relationship between upstream blocking and cold temperature extremes over North America in observations, reanalysis products (ERA-Interim and NARR), and RCMs (CanRCM4, CRCM5, HIRHAM5, and RCA4). Generalized extreme value distributions were fitted to winter minimum temperature (TNn) incorporating blocking frequency (BF) as a covariate, which is shown to have a significant influence on TNn. The magnitude of blocking influence in the RCMs is consistent with observations, but the spatial extent varies. CRCM5 and HIRHAM5 reproduce the pattern of influence best compared to observations. CanRCM4 and RCA4 capture the influence of blocking in British Columbia and the northeastern United States, but the extension of influence that is seen in observations and reanalysis into the southern United States is not evident. The difference in the 20-yr return value (20RV) of TNn between high and low BF in the Pacific Ocean indicates that blocking is associated with a decrease of up to 15°C in the 20RV over the majority of the United States and in western Canada. In northern North America the difference in the 20RV is positive as blocking is associated with warmer extreme cold temperatures. The 20RVs are generally simulated well by the RCMs.

1. Introduction

Extreme events have large impacts on both human and natural systems. It is important to understand large-scale circulation features that are associated with climate extremes and how well these relationships are simulated by climate models. It is often argued that regional climate models (RCMs) add value to lower-resolution global climate simulations by more skillfully representing extremes. The evaluation of relationships between extremes and circulation features is particularly interesting in RCMs because these circulation features can be located outside or near the edge of the model's domain. The relationship between these external circulation features and extremes allows us to evaluate how well the RCMs simulate these dynamically controlled aspects.

It is well established that atmospheric blocking, a disruption of the prevailing westerly flow, is associated with anomalous warm and cool temperatures. Atmospheric blocking in the North Pacific has both local (Pfahl and Wernli 2012) and downstream (Carrera et al. 2004; Favre and Gershunov 2006; Casola and Wallace 2007) impacts on North American temperatures, associated with either changes in the radiative balance or cold air advection, respectively (Pfahl and Wernli 2012). Warm extremes are associated with collocated blocking events, while blocking has an influence on remote cold minimum temperature anomalies (Carrera et al. 2004; Favre and Gershunov 2006; Casola and Wallace 2007; Pfahl and Wernli 2012). For example, blocking in the

Denotes Open Access content.

Corresponding author address: Kirien Whan, Pacific Climate Impacts Consortium, University of Victoria, Victoria, BC V8W3R4, Canada.
E-mail: kwhan@uvic.ca

DOI: 10.1175/JCLI-D-15-0493.1

Alaskan region is associated with warmer temperatures in western Alaska but a shift to cooler mean and extreme surface temperatures from Yukon to the Great Plains (Carrera et al. 2004). Furthermore, increased cyclonic activity in the northeast Pacific is associated with fewer Arctic air advections and fewer cold and extreme cold days in western North America, although the sign of the relationship changes into Mexico (Favre and Gershunov 2006). Alaskan ridging is associated with significantly more extreme cold days over much of the western and southern regions of the United States (Casola and Wallace 2007).

Previous research into the relationship between blocking and extremes used percentile-based definitions of extremes (Carrera et al. 2004; Favre and Gershunov 2006; Casola and Wallace 2007; Pfahl and Wernli 2012). The use of extreme value statistics is another approach that can be used to study statistically extreme events (Coles 2001). An extreme value framework has been used to study changes in extreme temperature (Bonsal et al. 2001; Wang et al. 2013) and precipitation (DeGaetano 2009; Whan and Zwiers 2016b) in North America. Nonstationary models have been used to examine the influence of covariates (such as blocking or soil moisture) on extreme temperature in Europe (Sillmann et al. 2011; Whan et al. 2015). In North America, a nonstationary generalized extreme value (GEV) framework has been used to explore the relationship between heat waves in Florida and indices of El Niño–Southern Oscillation (Keellings and Waylen 2015). To date, a GEV method has not been used to examine the relationship between blocking and temperature extremes in North America, and the need for further research in this area has been noted (Grotjahn et al. 2016). However, in Europe, nonstationary GEV distributions have been used to demonstrate the influence of Atlantic blocking on minimum temperatures in observations and global climate models (Sillmann et al. 2011) and the influence of the North Atlantic Oscillation and atmospheric blocking on hot spells (Photiadou et al. 2014).

There is high uncertainty about projected circulation changes (Shepherd 2014), so it is important to understand relationships between circulation patterns and temperature extremes in the current climate. Increased understanding of the observed relationships and the ability of models to simulate these relationships can increase certainty that projected changes have a physical basis and are not the result of model errors or biases. As such, it is also important to understand how well RCMs can simulate the observed relationship between atmospheric blocking and minimum temperature extremes in North America. We use a suite of RCMs from the Coordinated Regional Climate Downscaling Experiment (CORDEX) (Giorgi et al. 2009) that use surface and lateral boundary conditions derived from ERA-Interim (Diaconescu et al. 2015; Dee et al. 2011). The ability of RCMs to simulate circulation features can vary greatly (Li et al. 2015). A suite of RCMs in Europe was able to reproduce the pattern of the surface temperature response to Atlantic blocking, although the magnitude of the anomalies varied between models (Tourpali and Zanis 2013). Extreme value theory can be used to evaluate climate models by comparing the parameters of the GEV distribution between observed and modeled datasets (Casati and de Elía 2014). Here we evaluate the relationship between minimum temperature and blocking in four CORDEX generation RCMs using nonstationary GEV distributions.

2. Data and methods

a. Data

We focus on the monthly minima of daily minimum temperature (TNn) in North America over the winter [December–February (DJF)] months in 1989–2009. We use three observationally based products: one called ANUSPLIN+Livneh (McKenney et al. 2011; Livneh et al. 2013), ERA-Interim, and the North American Regional Reanalysis (NARR; Mesinger et al. 2006). The ANUSPLIN+Livneh dataset combines two high-resolution gridded datasets based on stations from Canada (McKenney et al. 2011) and the continental United States (Livneh et al. 2013). It should be noted that uncertainty in ANUSPLIN+Livneh is higher in regions where observations are sparse. See Whan and Zwiers (2016) for more details on this combined dataset. Surface temperature in reanalysis products is influenced directly by both observations and the model, so it is classified as a ''type B'' variable by Kalnay et al. (1996). As such, caution is required when interpreting surface temperature from the reanalysis products.

The observationally based datasets are compared with seven RCM simulations: the CCCma Regional Climate Model, version 4 (CanRCM4) and three variants of it (defined below), called CanRCM4noSN, CanRCM4022, and CanRCM4NCEP; as well as CRCM version 5 (CRCM5), RCA version 4 (RCA4), and HIRHAM version 5 (HIRHAM5). (Expansions are available online at http://www.ametsoc.org/PubsAcronymList.) A summary of information about the observed and modeled datasets can be found in Table 1. The RCM simulations have a common horizontal resolution (0.44°) on a rotated-pole grid (centered on 42.5°N, 83.0°W) and use lateral boundary conditions sourced from ERA-Interim, with two exceptions. One CanRCM4 simulation (CanRCM4022) has a higher horizontal resolution (0.22°), and another CanRCM4 simulation

TABLE 1. Details of observations, reanalysis products, and regional climate models. The institutes used are the Canadian Centre for Climate Modelling and Analysis (CCCma), the Université du Québec à Montréal (UQAM), the Canadian Forest Service (CFS), the National Centers for Environmental Prediction (NCEP), the University of Washington (UoW), the Danish Meteorological Institute (DMI), and the Swedish Meteorological and Hydrological Institute (SMHI).

	Institute	Original resolution (°)	Original dimensions (x, y)
ANUSPLIN+Livneh	CFS and UoW	0.08	1068,701
ERA-Interim	ECMWF	0.75	480, 241
NARR	NCEP	0.30	349, 277
CanRCM4	CCCma	0.44	155, 130
CanRCM4noSN	CCCma	0.44	155, 130
CanRCM4022	CCCma	0.22	310, 260
CanRCM4NCEP	CCCma	0.44	155, 130
CRCM5	UQAM	0.44	172, 160
HIRHAM5	DMI	0.44	155, 130
RCA4	SMHI	0.44	155, 130

(CanRCM4NCEP) has lateral boundary conditions derived from NCEP-2 (Kanamitsu et al. 2002). CanRCM4 (Scinocca et al. 2016) is run with spectral nudging for large scales, except for one version that has a free interior (CanRCM4noSN). CanRCM4 and CRCM5 (Zadra et al. 2008) are two Canadian RCMs that share the same dynamical core but with different physics schemes and different versions of the same land surface scheme, the Canadian Land Surface Scheme (CLASS; Verseghy 1991). Information about model physics can be seen in Table 2, and for further details on the differences among models see Scinocca et al. (2016) for CanRCM4, Zadra et al. (2008) for CRCM5, Samuelsson et al. (2011) for RCA4, and Christensen et al. (2006) for HIRHAM5.

Preprocessing of all datasets included the removal of ocean-based points (where required) and interpolation to the CanRCM4 0.44° rotated-pole grid, using bilinear interpolation from the climate data operators (Max Planck Institute 2013). While all CORDEX generation models use the same rotated-pole grid, the original dimensions of CRCM5 and the higher-resolution simulation (CanRCM4022) are larger than the final CanRCM4 grid (Table 1).

b. Methods

1) BLOCKING INDEX

Atmospheric blocking refers to a disruption of the prevailing westerly flow that is often associated with persistent ridging (Renwick and Wallace 1996; Rex 1950). Blocking occurs at high latitudes in the northeast Atlantic (270°–90°E) and Pacific (100°–240°E) Oceans, generally between 50° and 60°N in the Atlantic and between 60° and 70°N in the Pacific (Barriopedro et al. 2006). Atlantic blocking is prominent throughout the year, while for the Pacific sector blocking frequency is largest in winter (Cheung et al. 2013).

Atmospheric blocking is characterized in this study as per Tibaldi and Molteni (1990). The daily one-dimensional Tibaldi and Molteni (1990) index (TM90) classifies longitudes as either blocked or not blocked using midtroposphere meridional pressure gradients south [GHGS; Eq. (1)] and north [GHGN; Eq. (2)] of a central reference latitude (e.g., $\Phi_O = 60°\text{N}$). The GHGS is a measure of the zonal flow intensity at each longitude, and inclusion of the GHGN is required to exclude some nonblocked flows defined with only the GHGS (Barriopedro et al. 2006). Nonblocked flows occur when geopotential heights are lower at the central latitude compared to lower latitudes. In contrast, high geopotential heights at the central latitude compared to lower latitudes are indicative of a blocked flow. The gradients are defined as

$$\text{GHGS} = \left[\frac{Z(\Phi_O) - Z(\Phi_S)}{\Phi_O - \Phi_S}\right] \quad \text{and} \tag{1}$$

$$\text{GHGN} = \left[\frac{Z(\Phi_N) - Z(\Phi_O)}{\Phi_N - \Phi_O}\right]. \tag{2}$$

For the central latitudes we use $\Phi_O = 60°\text{N} \pm \delta$, the southern latitudes are $\Phi_S = 40°\text{N} \pm \delta$, and the northern latitudes are $\Phi_N = 80°\text{N} \pm \delta$, where $\delta = 5°, 0°, -5°$. These central reference latitudes have been used previously in global studies examining both Pacific and Atlantic blocking events. We calculate the GHGS and GHGN separately for three values of δ at each longitude from the five-day mean 500-hPa geopotential height Z of ERA-Interim (the RCMs' driving product). Use of five-day mean geopotential height anomalies ensures blocking events are of a sufficient length. These values of Φ are consistent with previous studies (Tibaldi and Molteni 1990; Shabbar et al. 2001), while other studies use small variations on these values (Barriopedro et al. 2006). At each time step, a given longitude is classified as blocked when, for at least one of the three values of δ,

TABLE 2. The physical parameterization schemes for each of the RCMs.

	Convection	Radiation	Microphysics	Planetary boundary layer
CanRCM4	Zhang and McFarlane (1995) and von Salzen et al. (2005)	Li and Barker (2005), Barker et al. (2008), and von Salzen et al. (2005)	Lohmann and Roeckner (1996), Rotstayn (1997), and Khairoutdinov and Kogan (2000)	Abdella and McFarlane (1997)
CRCM5	Kain and Fritsch (1990) and Kuo (1965)	Li and Barker (2005)	Sundqvist Berge et al. (1989)	Benoit et al. (1989) and Delage and Girard (1992)
HIRHAM5	Tiedtke (1989)	Fouquart and Bonnel (1980)	Tiedtke (1989) and Tompkins (2002)	Samuelsson et al. (2011)
RCA4	Kain and Fritsch (1990, 1993)	Savijärvi (1990) and Sass et al. (1994)	Rasch and Kristjánsson (1998)	Cuxart et al. (2000)

GHGS > 0 and GHGN < -10 meters per degree latitude. These thresholds are consistent across many studies (Tibaldi and Molteni 1990; Shabbar et al. 2001; Barriopedro et al. 2006; Diao et al. 2006).

We focus on blocking events occurring in the northeastern Pacific Ocean (EP; 160°E–110°W; Fig. 1a). We characterize blocking in this sector by an index of blocking frequency (BF), which is the percentage of days per month when any longitudes in the EP sector are classified as blocked. A BF of 10% in a 31-day month equates to approximately 3 blocked days, although it does not ensure that blocked days are consecutive. The monthly winter BF is 20% and the standard deviation is 20%. The mean winter BF at each longitude in ERA-Interim is generally consistent with previous definitions based on NCEP–NCAR reanalysis (Kalnay et al. 1996; Barriopedro et al. 2006), with the preferred blocking locations centered in the Atlantic and Pacific Oceans (Fig. 1b). The time series of winter mean BF (Fig. 1c) shows no significant trend over the relatively short study period.

Examples from two months that have high (Fig. 2a) and low (Fig. 2b) BF in the EP sector shows the typical flow and geopotential height anomalies under these two regimes. Under a nonblocked regime the positive geopotential height anomaly is located in the central Pacific midlatitudes with a westerly flow dominant over the majority of North America. When the EP sector is blocked, a positive geopotential height anomaly is located over the Alaskan region, which is associated with northerly flow over western Canada and the United States extending to around 35°N.

It is worth mentioning some of the shortcomings of the TM90 index. It has been noted that the use of the same reference latitudes throughout the hemisphere does not realistically reflect the spatial variability in the jet stream (Barriopedro et al. 2010). Furthermore, the one-dimensional nature of the index means it does not account for the extension and spatiotemporal propagation of blocking events (Barriopedro et al. 2010). Accordingly, other blocking indices have been developed in an attempt to overcome these limitations, such as the two-dimensional extension of the TM90 index (Scherrer et al. 2006). This two-dimensional TM90 index is calculated in a similar manner to the one-dimensional index, except that the central latitude is allowed to vary between 35° and 75°N in 2.5° increments, with the geopotential height gradients calculated over 15° bands north and south from the central latitude. As we allow three central latitudes from 55° to 65°N, the index used here can be thought of as a subset of the full two-dimensional TM90 index that focuses only on the upstream Alaskan blocking events that have been linked to minimum temperature extremes in previous work (e.g., Carrera et al. 2004). As a robustness check we repeated the analysis using a version of the two-dimensional index that was focused on the high latitudes in the northeastern Pacific. Results are largely similar for the majority of the continent, so we have chosen to use the more simple one-dimensional index.

2) GENERALIZED EXTREME VALUE ANALYSIS

The relationship between BF and minimum temperature in DJF is evaluated using extreme value theory (Coles 2001). The GEV distribution is used to model block maxima and can be described by three parameters: the location μ, which is similar to the mean; the scale σ, which is a measure of variability; and the shape ξ, which describes which distribution the data fit. Depending on ξ, the data fit one of the following distributions: the Gumbel if $\xi = 0$; the Frechet if $\xi > 0$, which has an unbounded tail on the right; or the Weibull if $\xi < 0$, which is bounded above. First the GEV distribution was fitted by the maximum likelihood method to the negative of DJF monthly TNn without covariates (M0).

Next, the influence of BF on TNn is quantified by the inclusion of a covariate in the nonstationary GEV models. The covariate (BF, designated z) is included on

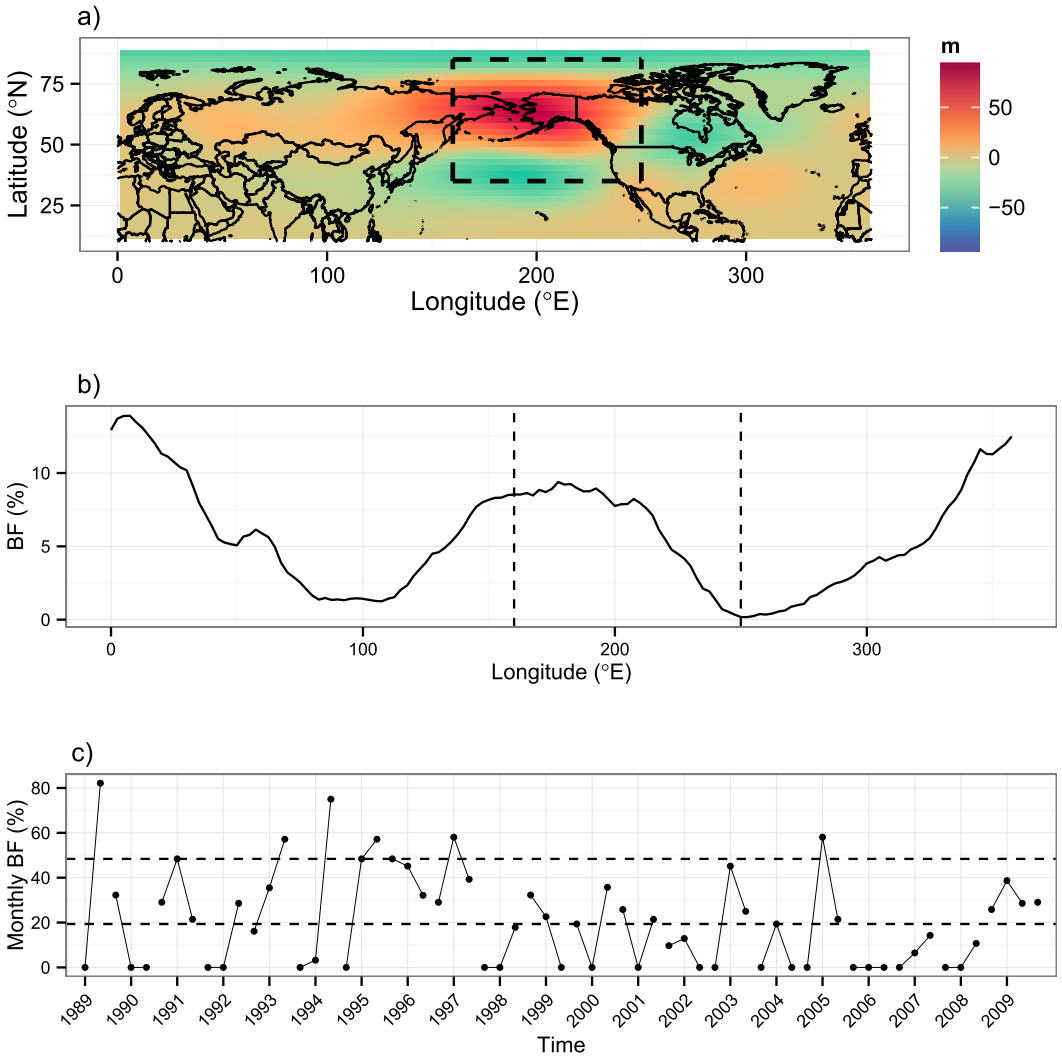

FIG. 1. (a) Five-day mean geopotential height anomalies (m) from ERA-Interim on days where any longitudes in EP sector (marked with dashed lines) are blocked. (b) Mean blocking frequency by longitude for winter months (1989–2009); dashed lines indicate the EP sector. (c) The time series of monthly winter (DJF with the year marker indicating January and other months excluded) blocking showing the percentage of days per month when any longitudes in the northeastern Pacific are blocked. Horizontal lines in (c) show the 90th and 50th percentiles of BF.

either the location parameter M1 or on both the location and scale parameters M2. Where a covariate is included on the location parameter, it varies linearly with the covariate so that $\mu(z) = \beta_0 + \beta_1 z$. Where a covariate is included on the scale parameter, it is allowed to vary log-linearly with the covariate to ensure the scale parameter remains positive, so that $\log(\sigma) = \gamma_0 + \gamma_1 z$. We assume that the shape parameter is constant and does not vary with the covariate. The slope of the covariate gives an indication of the magnitude of the influence per unit of the covariate, in this case per 1% change in blocking. Results are presented in terms of a 10% change in blocking frequency. After fitting the GEV to the negative of TNn, the sign of the location parameter μ and thus the coefficient on the covariate β_1 are reversed so the results can be presented in physically consistent values. The fit of the GEV (M2) to winter TNn in North America is tested with the application of a standard Kolmogorov–Smirnov goodness-of-fit (KS) test at the $p < 0.05$ significance level. In the nonstationary model, the KS test is applied to data that are first transformed to a standard Gumbel distribution, conditional on the fitted parameter values (Coles 2001; Zhang et al. 2010).

The likelihood-ratio test (LRT) is used to evaluate whether the introduction of covariates have a significant influence. The LRT compares nested GEV models (i.e., M1 is M2 with γ_1 set to zero and M0 is M1 with β_1 set

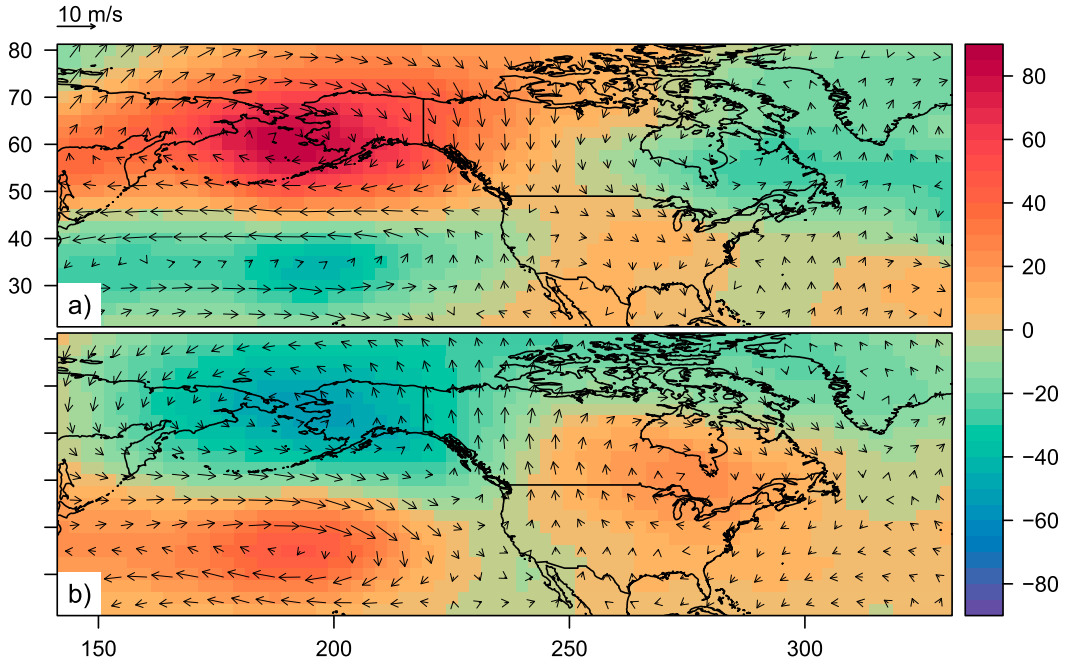

FIG. 2. Vector wind (m s^{-1}; arrows) and 500-hPa geopotential height anomalies (m; colors) in composite average months with (a) BF greater than one standard deviation above the mean (high BF) and (b) BF greater than one standard deviation below the mean (low BF).

to zero). The LRT uses a test statistic [Eq. (3)] to compare the log likelihood of two nested models where, for example, l^0 is the log likelihood of M0 and l^1 is the log likelihood of M2:

$$T = 2(l^1 - l^0). \tag{3}$$

The statistic T is asymptotically χ^2_q distributed with q degrees of freedom, where q is the difference in the number of free parameters between the models (in the example given, $q = 2$). The more simple model is rejected at significance level α if T is larger than the $1 - \alpha$ quantile of the χ^2_q distribution (Zhang et al. 2010; Sillmann et al. 2011). We compare M0 with M2 to find where BF has a significant influence on minimum temperature. Then, for locations where the influence of the covariate is significant, we compare M1 with M2 to describe where BF significantly alters both the location and scale parameters.

GEV parameters are averaged on a regional basis. The effective 20-yr return values (20RVs) are a cold temperature event that we expect to occur with a probability of 0.05 or 1/20 years, given a particular value of the covariate (e.g., low or high BF). These are calculated at each pixel. One thousand random draws from GEV distributions with these regionally averaged GEV parameters adjusted for no blocking and average (50th percentile) and high (90th percentile) BF are used to reproduce TNn probability density function distributions.

All analysis is conducted in the R statistical computing environment (R Development Core Team 2014), and the GEV analysis uses the extRemes package (Gilleland 2014).

3. Results

a. *Observed influence of eastern Pacific blocking on TNn*

Observed (ANUSPLIN+Livneh, ERA-Interim, and NARR) monthly winter TNn minima fit the GEV distribution well across most of North America (Figs. 3a–c). The percentage of pixels failing the KS test is smaller than the expected 5%, with values between 5% in ERA-Interim and 10% in ANUSPLIN+Livneh and NARR. Most of these pixels are located in central and eastern Canada in areas where in situ observations are sparse.

Blocking has a significant influence on North American TNn, as the nonstationary model (M2) is selected over most of the continent (Figs. 3a–c). The observed datasets generally agree on the areas under the influence of blocking. In the southwestern United States and northeastern Canada, the inclusion of the covariate on the scale parameter significantly improves the fit of the GEV; however, there is less agreement between observationally based datasets on the extent of this influence, particularly in northeastern Canada. In ANUSPLIN+Livneh and ERA-Interim there are

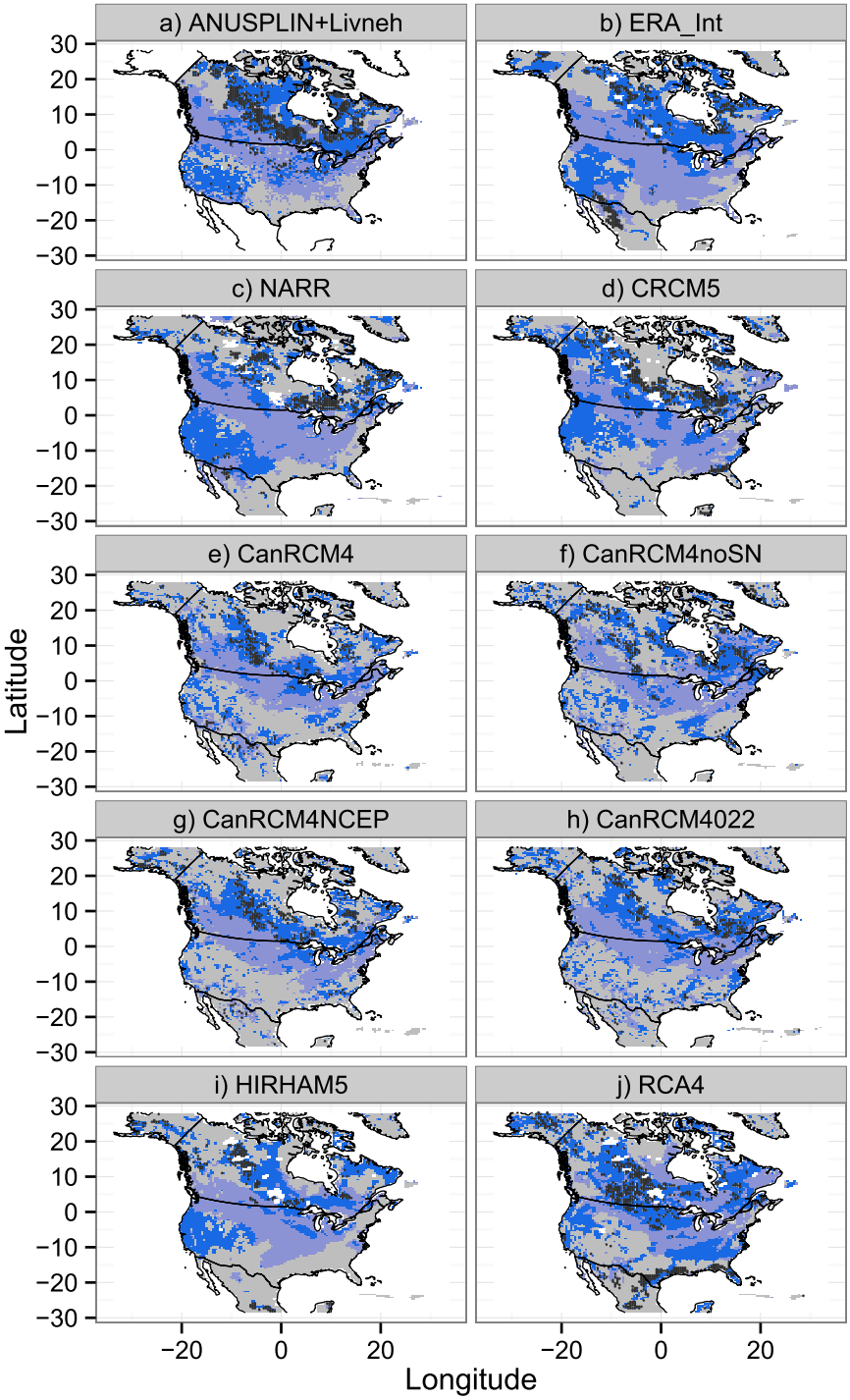

FIG. 3. Results of the likelihood ratio test showing where BF has a significant influence on minimum temperature (light and dark blue) and where blocking significantly influences both the location and scale parameters (dark blue) in (a) ANUSPLIN+Livneh, (b) ERA-Interim, (c) NARR, (d) CRCM5, (e) CanRCM4, (f) CanRCM4noSN, (g) CanRCM4NCEP, (h) CanRCM4022, (i) HIRHAM5, and (j) RCA4. Locations where the KS test showed the GEV is not a good fit for winter monthly TNn are indicated with dark gray dots.

large homogeneous regions in the northeast where the scale parameter appears to be influenced by blocking, while in NARR this region is more fragmented (Figs. 3a–c).

The slope of the covariate on the location parameter indicates that a higher BF is associated with lower minimum temperatures across most of the continent, excluding the southwest (Figs. 4a–c). Blocking is associated with increased TNn variability in the south, particularly in the southwest, and decreased variability in the north (Figs. 5a–c). The pattern of blocking influence on the scale parameter does not match exactly to that of the location parameter, particularly in eastern North America. In the southeast United States, for example, increased blocking is associated with lower temperatures and more variability in minimum temperatures. In contrast, in western Canada increased blocking is associated with both lower temperature and less variability. Based on these patterns, three regions are defined for further analysis. In RegPP and RegNN, blocking has a positive (RegPP) or negative (RegNN) influence on both parameters, while in RegNP blocking has a negative influence on the location parameter and the influence on the scale parameter is mixed (Fig. 4a).

On the continental scale, there is good agreement between the GEV parameters in ERA-Interim and NARR with ANUSPLIN+Livneh (Fig. 6). The spatial correlation of the location parameters in the reanalysis products and observations is high ($r > 0.9$), and the amplitudes of the variations in all parameters are reasonably well matched to observations. The influence of blocking on the location parameter is larger in ERA-Interim and NARR compared to observations, while the blocking influence on the scale parameter is more realistic (Fig. 6).

Regionally averaged GEV parameters demonstrate biases in the location parameter μ between the observationally based datasets of up to 6°C in RegNN and RegPP (Tables 3 and 4) and 4°C in RegNP (Table 5). The reanalysis products are warmer than ANUSPLIN+Livneh in all regions, although the cause of this difference remains unresolved. Previous comparison of the coldest day of the year also found widespread warm bias in NARR and ERA-Interim (Whan and Zwiers 2016a). However, there is agreement between observationally based datasets on the regionally averaged scale parameter σ and on the slope of the covariates β_1 and γ_1. In RegNN, blocking is associated with up to a 1.12°C decrease in TNn per 10% change in BF. The positive influence of blocking on the location parameter in RegPP is smaller, a 0.34°C increase in TNn for ANUSPLIN+Livneh and reanalysis products (Table 4). In RegNP increased blocking is associated with a decrease in the location parameter in all datasets (up to −0.9°C in NARR).

Averaged over RegNN, the negative influence of blocking on the scale parameter γ_1 is small but significantly different than zero, at −0.25° to −0.33°C (Table 3). In RegPP there is a positive influence of blocking on TNn variability. On average, blocking is associated with a 0.41°C increase in the variability of TNn per 10% increase in BF. In RegNP, there is a −0.15°–0.09°C change in γ_1 per 10% change in BF, with a negative slope in ANUSPLIN+Livneh, an insignificant positive slope in ERA-Interim and a significant positive slope in NARR (Table 5).

The influence of blocking can be seen clearly in the PDFs of TNn reconstructed from regionally averaged GEV parameters (Figs. 7, 8, and 9). In RegNN TNn is well separated according to blocking regime. Most of this separation occurs in the warmer part of the distribution, so that temperatures above −15°C are rarely experienced under a high blocking regime. The separation of distributions according to blocking regime is less consistent in RegNP (Fig. 8). In all datasets the cold tail of the distribution is well separated by blocking regime, although NARR has the largest differences. The influence of the scale parameter is evident, as the distribution of ANUSPLIN+Livneh under high blocking is narrower and well separated on the warm tail, while the reanalysis products are wider with little separation at the warm tail. The influence of blocking on the variability of RegPP TNn can be seen in Fig. 9. Under a high blocking regime, the distribution is much wider with a higher probability of TNn values greater than 0°C, while when there is no blocking the distribution of TNn in RegPP is narrow with a low probability of TNn greater than 0°C (Fig. 9).

The difference in the 20-yr return values between high (90th percentile) and low (10th percentile) blocking regimes shows the influence that blocking has on extreme cold events. These return values combine the previous information, are informative from a user perspective, and show the regions where blocking has the largest influence (Fig. 10). Over the continental United States high blocking generally has a negative influence on TNn. On the continental scale there is good agreement in the 20RV between reanalysis products and ANUSPLIN+Livneh as the spatial correlation is moderately large ($r > 0.6$), the overall bias is small (<4°C), and the amplitude of the variations is realistic (Fig. 6). In all observationally based datasets high blocking is associated with up to a 15°C decrease in TNn, compared to low blocking. The negative difference in return values in the southwest, despite a positive slope in the covariate on the location parameter, is due to the influence of the scale parameter and the increased variability under a blocking regime. The regions with the largest differences in 20RV between blocking regimes are centered around the Pacific Northwest and central United

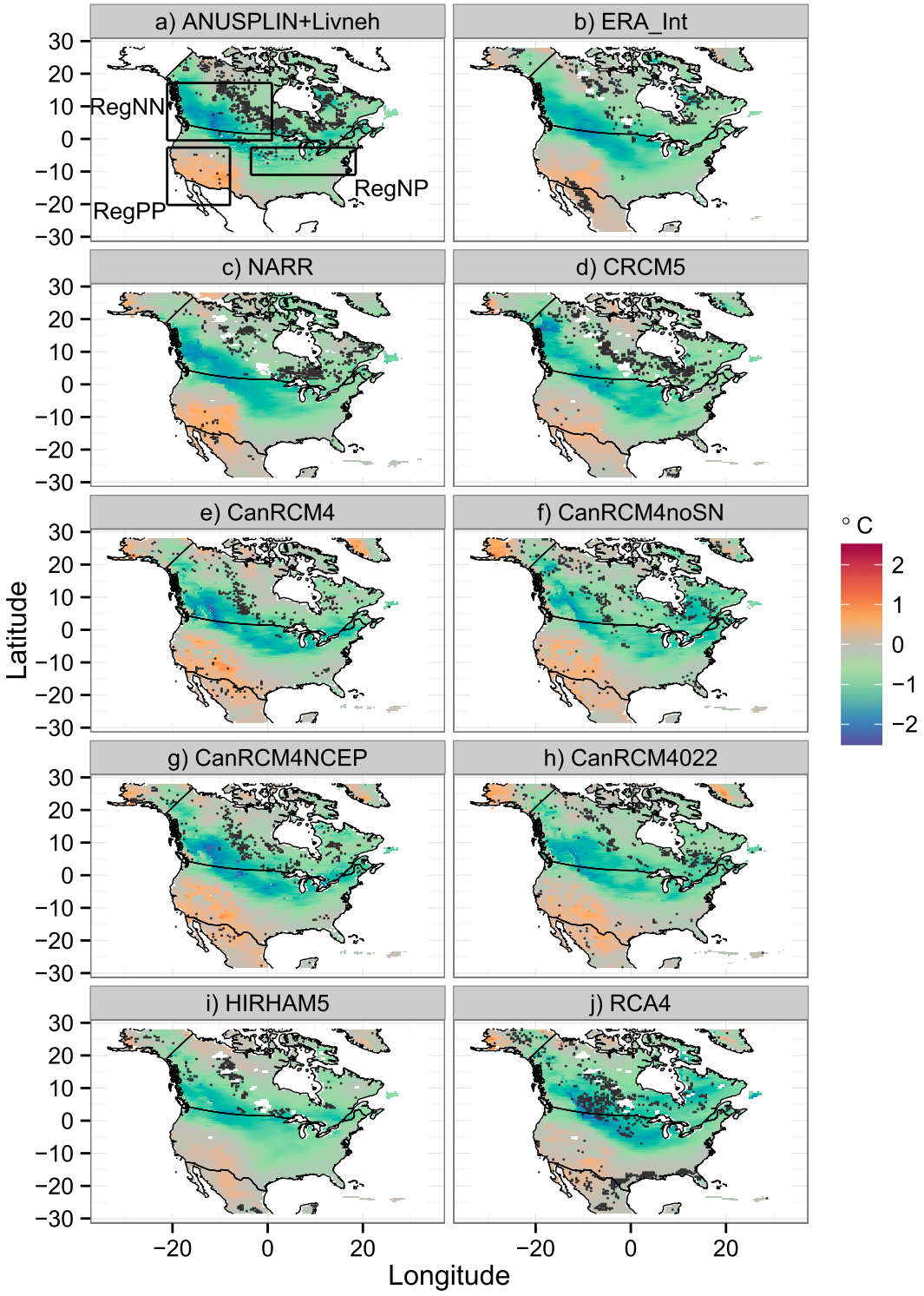

FIG. 4. The slope of the covariate on the location parameter (degrees Celsius per 10% change in BF) from M2 in (a) ANUSPLIN+Livneh, (b) ERA-Interim, (c) NARR, (d) CRCM5, (e) CanRCM4, (f) CanRCM4noSN, (g) CanRCM4NCEP, (h) CanRCM4022, (i) HIRHAM5, and (j) RCA4. Pixels where the GEV is not a good fit for winter TNn are marked in gray. Regions of positive (RegPP), negative (RegNN), and mixed (RegNP) influence are outlined.

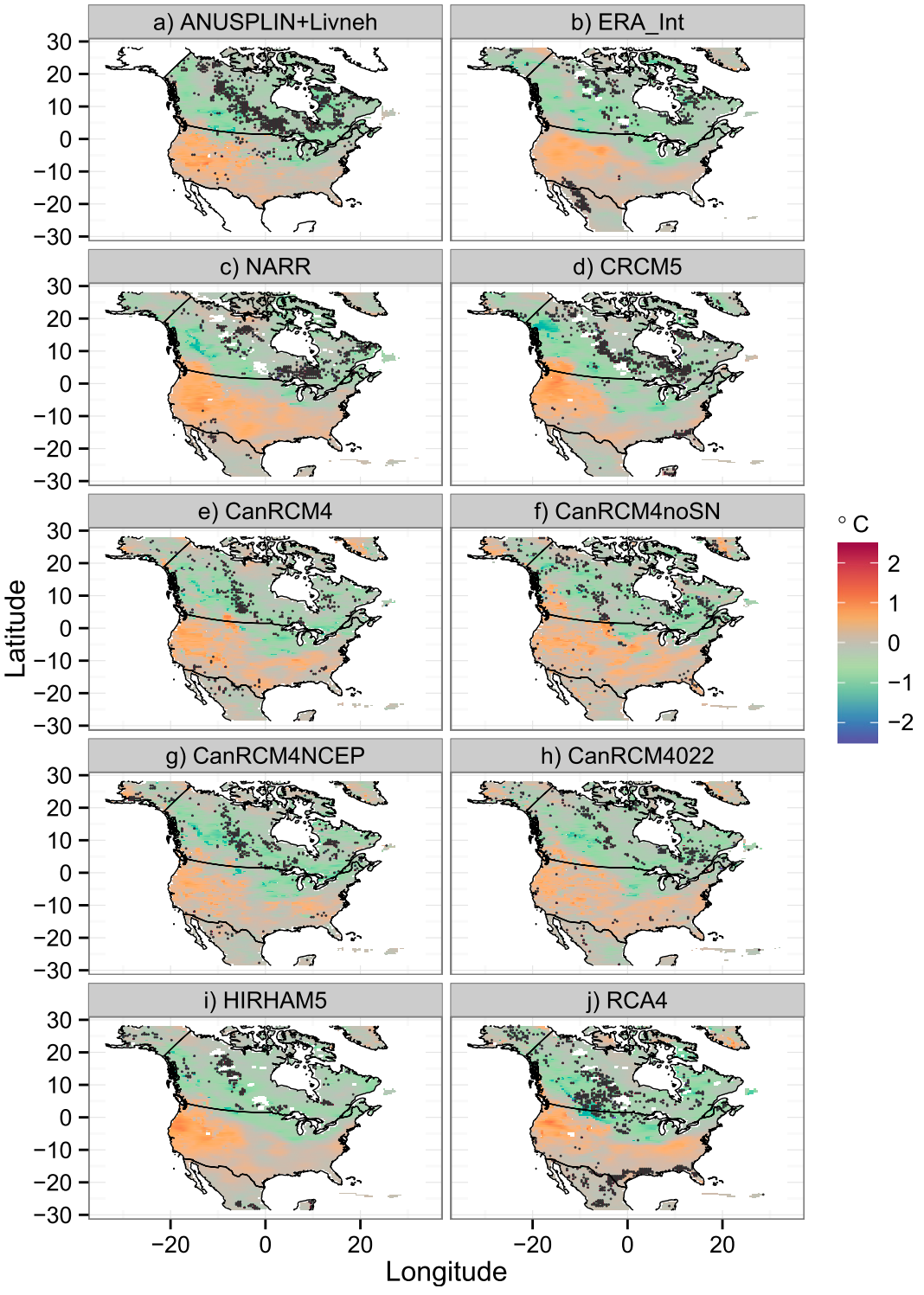

FIG. 5. The slope of the log-transformed scale parameter (degrees Celsius per 10% change in BF) from M2 in (a) ANUSPLIN+Livneh, (b) ERA-Interim, (c) NARR, (d) CRCM5, (e) CanRCM4, (f) CanRCM4noSN, (g) CanRCM4NCEP, (h) CanRCM4022, (i) HIRHAM5, and (j) RCA4. Pixels where the GEV is not a good fit for winter TNn are marked in gray.

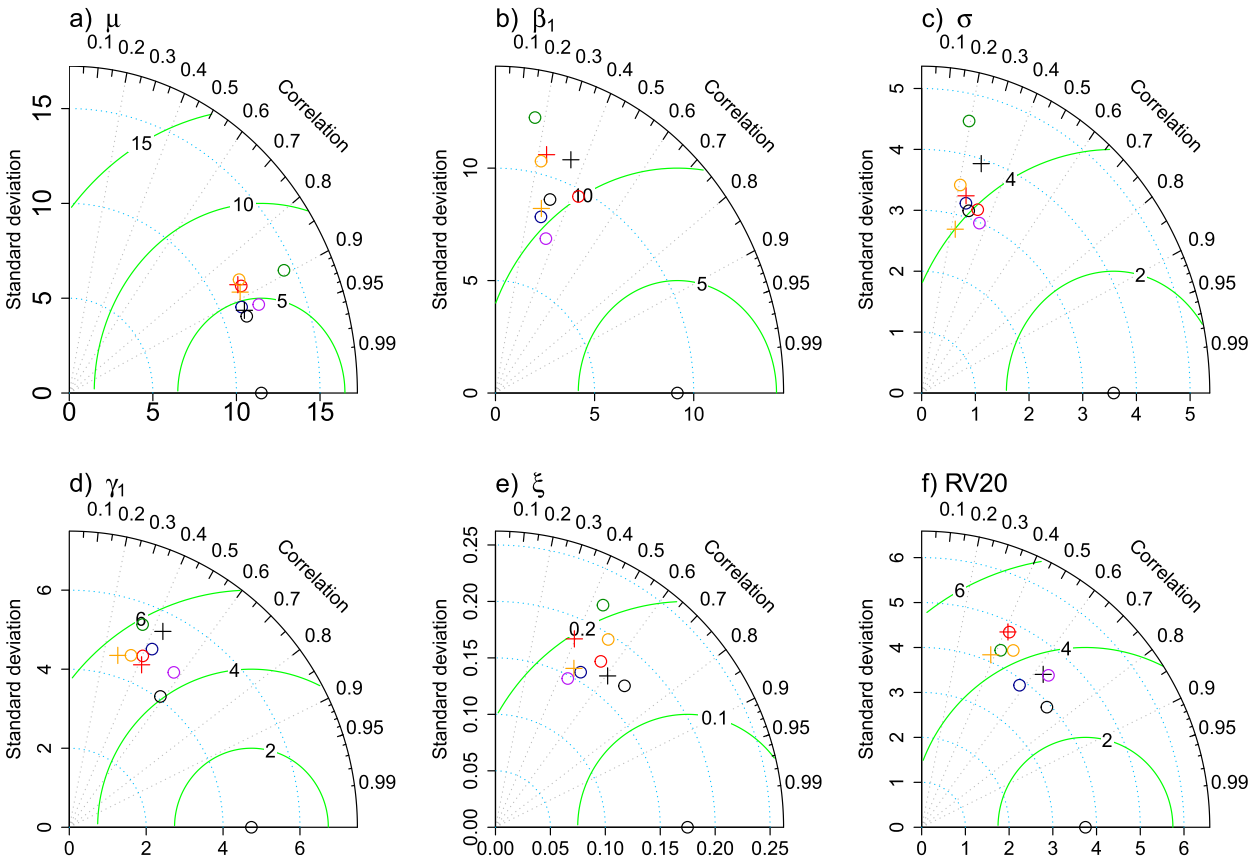

FIG. 6. Taylor diagrams showing the standard deviation (blue arcs), the root-mean-square error (green arcs), and the correlation (black outer arc) of (a) the location parameter, (b) the slope of the covariate on the location parameter, (c) the scale parameter, (d) the slope of the log-transformed scale parameter, (e) the shape parameter, and (f) the difference in 20RV between high and low blocking regimes, in reanalysis products (NARR = black cross, and ERA-Interim = black circle) and RCMs (CanRCM4 = red circle, CanRCM4noSN = orange cross, CanRCM4022 = red cross, CanRCM4NCEP = orange circle, CRCM5 = blue circle, RCA4 = green circle, and HIRHAM5 = purple circle) compared to ANUSPLIN+Livneh.

States, although again the reanalysis products have a much more spatially coherent signal compared to ANUSPLIN+Livneh. There is a change of sign in western Alaska and Mexico as differences in the 20-yr return level between high and low BF are positive, indicating that blocking is associated with warmer extreme cold temperatures in these regions.

b. *Evaluation of regional climate model simulations*

The fit of the GEV to winter TNn in the RCMs is generally consistent with observations, as the majority of pixels failing the KS test are located in central Canada (Fig. 3). Furthermore, the percentage of pixels failing the KS test is comparable to observed, as between 3% and 9% of pixels are not a good fit. Compared to the observationally based datasets, all simulations except HIRHAM5 have an additional region failing the KS test in the southeast United States along the Gulf of Mexico. RCA4 has the largest percentage (9%) of land area where the GEV is not a good fit, with most of these points located in southern-central Canada and the southeast United States (Fig. 3j). It should be noted that these rejection rates are consistent with the significance level (i.e., the expected rate of false rejections when the GEV fits well) that was specified for the KS test. Also, to the extent that TNn exhibits spatially organized behavior, it is not unexpected that the rejection of the null hypothesis that the GEV fits well should occur in a spatially organized manner.

The pattern of blocking influence on TNn in the RCMs is generally consistent with the observed datasets (Fig. 3). Only HIRHAM5 and CRCM5 capture the extension of blocking influence on the location and scale parameters in the southwest, although HIRHAM5 does not capture the significant influence in western Canada (Fig. 3). All CanRCM4 simulations simulate the significant influence of blocking extending from British Columbia into the United States but do not simulate the extension of influence to the south and underestimate

TABLE 3. Regionally averaged GEV parameters in RegNN from M2 where a nonstationary model was selected as the best model. Confidence intervals from a single-sample t test ($p < 0.05$) are noted in parentheses.

	μ	β_1	σ	γ_1
ANUSPLIN+Livneh	−26.9 (−27.43, −26.36)	−1.02 (−1.07, −0.98)	6.1 (5.90, 6.29)	−0.32 (−0.34, −0.29)
ERA-Interim	−22.58 (−23.03, −22.13)	−1.06 (−1.13, −0.99)	5.91 (5.66, 6.16)	−0.33 (−0.35, −0.31)
NARR	−21.48 (−21.93, −21.03)	−1.12 (−1.16, −1.07)	6.2 (5.98, 6.42)	−0.25 (−0.28, −0.22)
CanRCM4	−27.42 (−27.84, −26.99)	−1.03 (−1.08, −0.99)	6.18 (6.04, 6.31)	−0.27 (−0.29, −0.24)
CanRCM4noSN	−27.96 (−28.41, −27.52)	−0.91 (−0.96, −0.87)	5.97 (5.83, 6.10)	−0.12 (−0.14, −0.09)
CanRCM4022	−28.26 (−28.63, −27.89)	−1.04 (−1.06, −1.02)	5.99 (5.92, 6.06)	−0.24 (−0.26, −0.22)
CanRCM4NCEP	−26.11 (−26.54, −25.68)	−0.98 (−1.02, −0.93)	6.23 (6.05, 6.41)	−0.25 (−0.28, −0.22)
CRCM5	−27.96 (−28.40, −27.52)	−1.13 (−1.20, −1.06)	6.75 (6.52, 6.98)	−0.34 (−0.37, −0.31)
HIRHAM5	−23.43 (−23.99, −22.86)	−0.95 (−1.02, −0.89)	6.22 (5.95, 6.49)	−0.29 (−0.32, −0.25)
RCA4	−26.52 (−27.15, −25.88)	−1.18 (−1.30, −1.06)	6.86 (6.45, 7.26)	−0.39 (−0.44, −0.35)

the influence of blocking on the TNn variability in southwestern North America (Figs. 3e,f). This indicates that the inability of the model to simulate the significant influence of blocking on TNn does not stem from the nesting strategy, lateral boundary conditions, or horizontal resolution and is instead likely related to the physics packages used in the RCM. In RCA4, BF has a significant influence on both the location and scale parameters in the southeast United States, which is not evident in the observations, and it does not simulate the significant influence of blocking in southwestern North America (Fig. 3j).

On the continental scale the RCMs simulate the location, scale, and shape parameters well compared to ANUSPLIN+Livneh (Fig. 6). Some instances where one or more models stand out from the others are noted. The RMSE in all GEV parameters in RCA4 compared to observations is larger than most other products. The amplitude of variations in the influence of blocking on the location parameter in CanRCM4 is somewhat larger than observed and more similar to the reanalysis products. The spatial correlation between the blocking influence on the scale parameter in HIRHAM5 and ANUSPLIN+Livneh is high and similar to that of ERA-Interim and ANUSPLIN+Livneh (Fig. 6).

In RegNN and RegPP, the estimated location parameter is replicated well in the RCMs compared to observationally based datasets (Fig. 4). In RegNN, CRCM5 and the CanRCM4 simulations have a similar location parameter to ANUSPLIN+Livneh, although CanRCM4NCEP is 1°C cooler than observations and the other simulations are around 1°C warmer. Previous work has shown that there are significant biases in CanRCM4 annual TNn compared to ANUSPLIN+Livneh, with significantly cooler temperatures in the Pacific Northwest and warmer temperatures east of the mountains in central Canada (Whan and Zwiers 2016a). The similarity between CanRCM4 simulations and observations here is likely due to the averaging of the positive and negative biases in each half of RegNN. The location parameters for HIRHAM5 and RCA4 in RegNN are more similar to reanalysis products (Table 3). In RegPP, all CanRCM4 simulations have a similar location parameter to observations, although somewhat cooler, consistent with the cool bias in annual TNn in the southwestern United States (Whan and Zwiers 2016a). CRCM5, HIRHAM5, and RCA4 are similar to reanalysis products with a warm bias compared to ANUSPLIN+Livneh (Table 4). In RegNP, all RCMs are warmer than ANUSPLIN+Livneh. The CanRCM4 and CRCM5 simulations are similar to reanalysis products, while HIRHAM5 and RCA4 have the largest warm bias, up to 8°C in RCA4.

In RegNN, the average influence of BF on the location parameter in the RCMs is similar to observed, as blocking results in a 0.91°–1.18°C decrease in TNn per 10% increase in BF. Two models run without spectral nudging, CRCM5 and CanRCM4noSN, which over- and underestimate the strength of the blocking influence, respectively, while HIRHAM5 also slightly underestimates the relationship (Table 3). In RegPP, the influence of blocking on the location parameter is somewhat larger than observed in CanRCM4, CanRCM4noSN, and CRCM5 but smaller than observed in CanRCM4NCEP, HIRHAM5, and RCA4. The influence of blocking on the location parameter in RegNP is too strong compared to all observationally based datasets in CanRCM4, CanRCM4NCEP, and CRCM5.

Similar to the observationally based datasets, in RegNN the influence of blocking on the scale parameter is small but significant in all simulations (Table 3). In RegPP, all RCMs simulate the significant positive influence of blocking on the scale parameter. In CanRCM4, CRCM5, and RCA4 blocking is associated with a 0.31°–0.4°C increase in TNn variability per 10% increase in BF, comparable to observations. In HIRHAM5 the influence of blocking on the scale parameter is too large, with a 0.55°C increase in TNn variability per 10% increase in BF (Table 4). The mixed signal in the sign of the covariate on the scale parameter in RegNP is also seen in the RCMs

TABLE 4. As in Table 3, but for RegPP.

	μ	β_1	σ	γ_1
ANUSPLIN+Livneh	−11.23 (−11.82, −10.65)	0.34 (0.32, 0.36)	1.96 (1.90, 2.01)	0.41 (0.39, 0.42)
ERA-Interim	−7.46 (−7.94, −6.98)	0.19 (0.17, 0.21)	1.72 (1.68, 1.76)	0.31 (0.30, 0.33)
NARR	−5.80 (−6.26, −5.34)	0.34 (0.32, 0.35)	1.82 (1.79, 1.86)	0.38 (0.36, 0.40)
CanRCM4	−11.44 (−12.07, −10.81)	0.36 (0.33, 0.39)	2.61 (2.53, 2.68)	0.32 (0.30, 0.35)
CanRCM4noSN	−13.30 (−14.13, −12.46)	0.30 (0.27, 0.32)	2.78 (2.68, 2.89)	0.34 (0.32, 0.37)
CanRCM4022	−13.43 (−14.31, −12.55)	0.28 (0.25, 0.32)	2.67 (2.56, 2.77)	0.32 (0.29, 0.35)
CanRCM4NCEP	−14.69 (−15.52, −13.85)	0.09 (0.07, 0.11)	2.76 (2.69, 2.83)	0.40 (0.38, 0.42)
CRCM5	−9.78 (−10.55, −9.01)	0.36 (0.32, 0.39)	2.56 (2.44, 2.67)	0.31 (0.28, 0.34)
HIRHAM5	−6.82 (−7.36, −6.27)	0.03 (0.02, 0.05)	1.85 (1.79, 1.90)	0.55 (0.53, 0.57)
RCA4	−7.32 (−8.17, −6.46)	0.10 (0.08, 0.12)	2.38 (2.23, 2.53)	0.30 (0.27, 0.33)

(Fig. 5). CanRCM4, CanRCM4NCEP, CRCM5, and HIRHAM5 reproduce the sign and magnitude of the slope compared to ANUSPLIN+Livneh, despite a disagreement between the driving model (ERA-Interim) and observations. CanRCM4noSN agrees with the driving model, while the spectrally nudged CanRCM4 does not. The improvement compared to observations in the downscaled run over ERA-Interim may demonstrate the added value of the RCMs, although more analysis is necessary given the positive slope in the highest resolution model-based products (NARR and CanRCM4022). Although care should be taken in the interpretation of these regional means, there is some value in the comparison, particularly for the CanRCM4 simulations. The lack of agreement between simulations of the same model is interesting as it suggests the relationship between TNn and blocking in this region is not only dependent on the physics packages of the RCM.

The influence of blocking on the PDFs of TNn in RegNN is generally consistent with the observed datasets (Fig. 7). In RegPP the observationally based datasets separate the PDFs of the three blocking regimes reasonably well at the warm end of the distribution. This separation is less evident in the RCMs, particularly for no-blocking and mean-blocking regimes in CanRCM4noSN and RCA4 and for the mean and blocking regimes in HIRHAM5 (Fig. 9). The PDF of TNn when BF is high is positively skewed in all CanRCM4 simulations, similarly to NARR (Fig. 9). In RegNP the distribution of TNn when BF is high is well reproduced by HIRHAM5 and CRCM5 compared to ANUSPLIN+Livneh, while the TNn distributions of CanRCM4 are too wide and negatively skewed (Fig. 8).

The 20RV difference between high and low blocking is generally well simulated by the RCMs, although there are differences compared to observations for some regions and models (Figs. 6 and 10). HIRHAM5 and CRCM5 generally capture the spatial extent and magnitude of the largest differences well compared to both observations and reanalysis (Fig. 6). The CanRCM4 simulations do not reproduce the magnitude and extent of the differences in the Pacific Northwest well, as the extent of the largest differences in the 20RVs is much reduced compared to the reanalysis products (Fig. 10). All CanRCM4 simulations and RCA4 have a region in the southeastern United States where the magnitude of the difference between blocking regimes is large. This region is evident in ERA-Interim but is of a smaller magnitude.

4. Discussion and conclusions

We examined the influence of northeastern Pacific blocking frequency (BF) on the winter monthly minima

TABLE 5. As in Table 3, but for RegNP.

	μ	β_1	σ	γ_1
ANUSPLIN+Livneh	−14.64 (−14.92, −14.35)	−0.81 (−0.86, −0.76)	4.4 (4.20, 4.60)	−0.15 (−0.18, −0.12)
ERA-Interim	−10.9 (−11.17, −10.63)	−0.86 (−0.88, −0.84)	4.08 (4.01, 4.16)	−0.08 (−0.10, −0.06)
NARR	−10.94 (−11.20, −10.68)	−0.9 (−0.91, −0.88)	4.13 (4.06, 4.20)	0.09 (0.07, 0.11)
CanRCM4	−11.64 (−11.98, −11.30)	−0.97 (−1.00, −0.94)	5.25 (5.07, 5.42)	−0.18 (−0.22, −0.15)
CanRCM4noSN	−11.63 (−11.94, −11.32)	−0.89 (−0.93, −0.84)	4.33 (4.20, 4.46)	0.16 (0.13, 0.18)
CanRCM4022	−11.66 (−12.06, −11.26)	−0.81 (−0.84, −0.79)	4.1 (3.95, 4.26)	−0.02 (−0.05, 0.01)
CanRCM4NCEP	−15.93 (−16.32, −15.54)	−0.95 (−0.97, −0.93)	4.97 (4.87, 5.06)	−0.27 (−0.29, −0.25)
CRCM5	−11.24 (−11.58, −10.89)	−0.96 (−0.99, −0.93)	5.05 (4.89, 5.21)	−0.18 (−0.21, −0.15)
HIRHAM5	−9.69 (−9.94, −9.44)	−0.72 (−0.73, −0.71)	4.18 (4.12, 4.25)	−0.09 (−0.11, −0.07)
RCA4	−7.35 (−7.66, −7.04)	−0.89 (−0.92, −0.86)	4.07 (3.90, 4.23)	−0.02 (−0.05, 0.01)

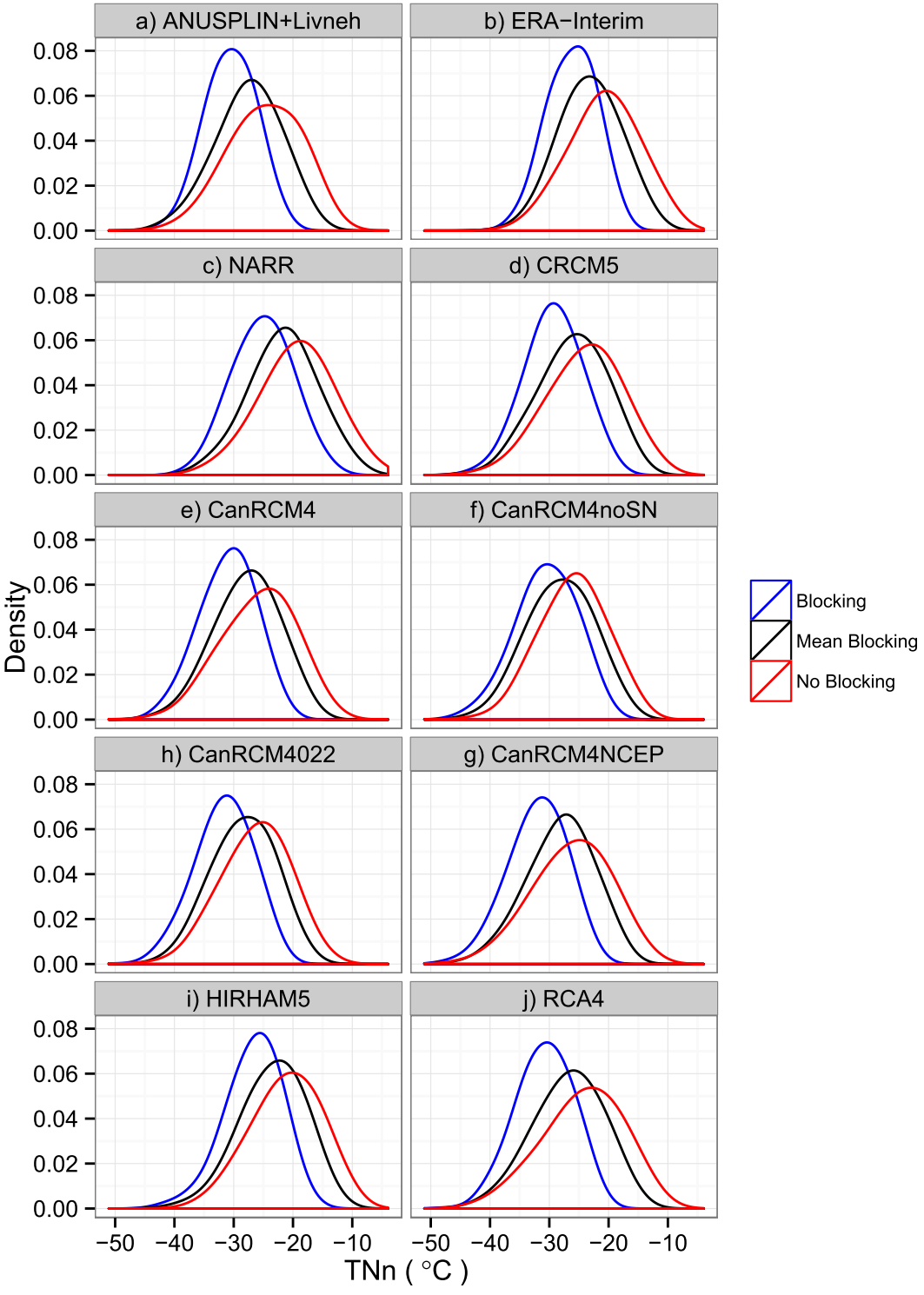

FIG. 7. Probability density functions of RegNN TNn estimated from average GEV parameters in M2 with no blocking (red), 6 days of blocking (50th percentile, black) and 16 days blocking (90th percentile, blue). Distributions are plotted for each dataset (a) ANUSPLIN+Livneh, (b) ERA-Interim, (c) NARR, (d) CRCM5, (e) CanRCM4, (f) CanRCM4noSN, (g) CanRCM4NCEP, (h) CanRCM4022, (i) HIRHAM5, and (j) RCA4.

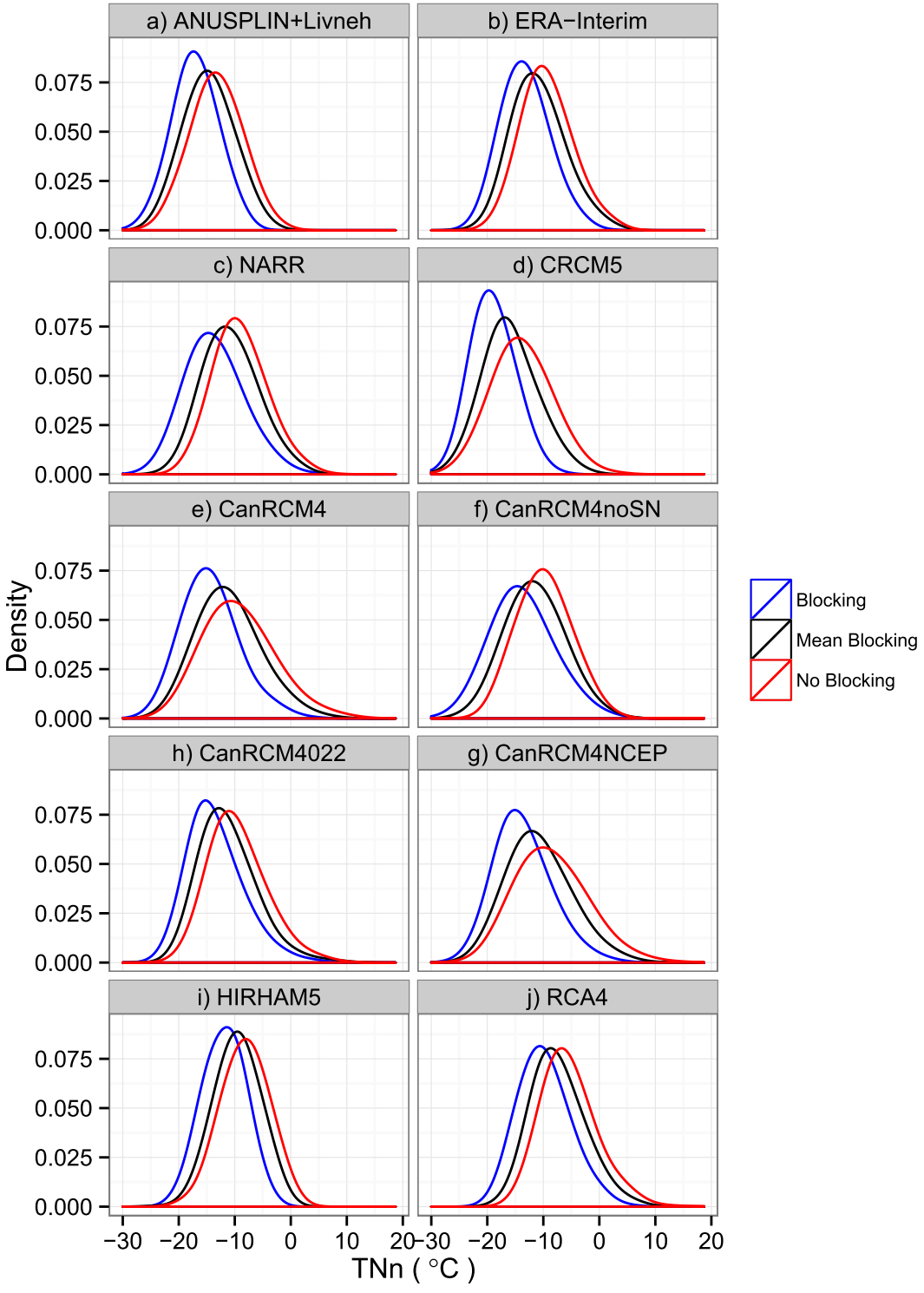

FIG. 8. As in Fig. 7, but for RegNP TNn.

of minimum temperature. We find that the inclusion of blocking frequency as a covariate in the GEV model significantly improves its fit over the majority of North America, demonstrating the extent of the significant influence blocking has on extreme minimum temperatures. In northern Canada and the southwestern United States blocking significantly influences both the location and scale parameters.

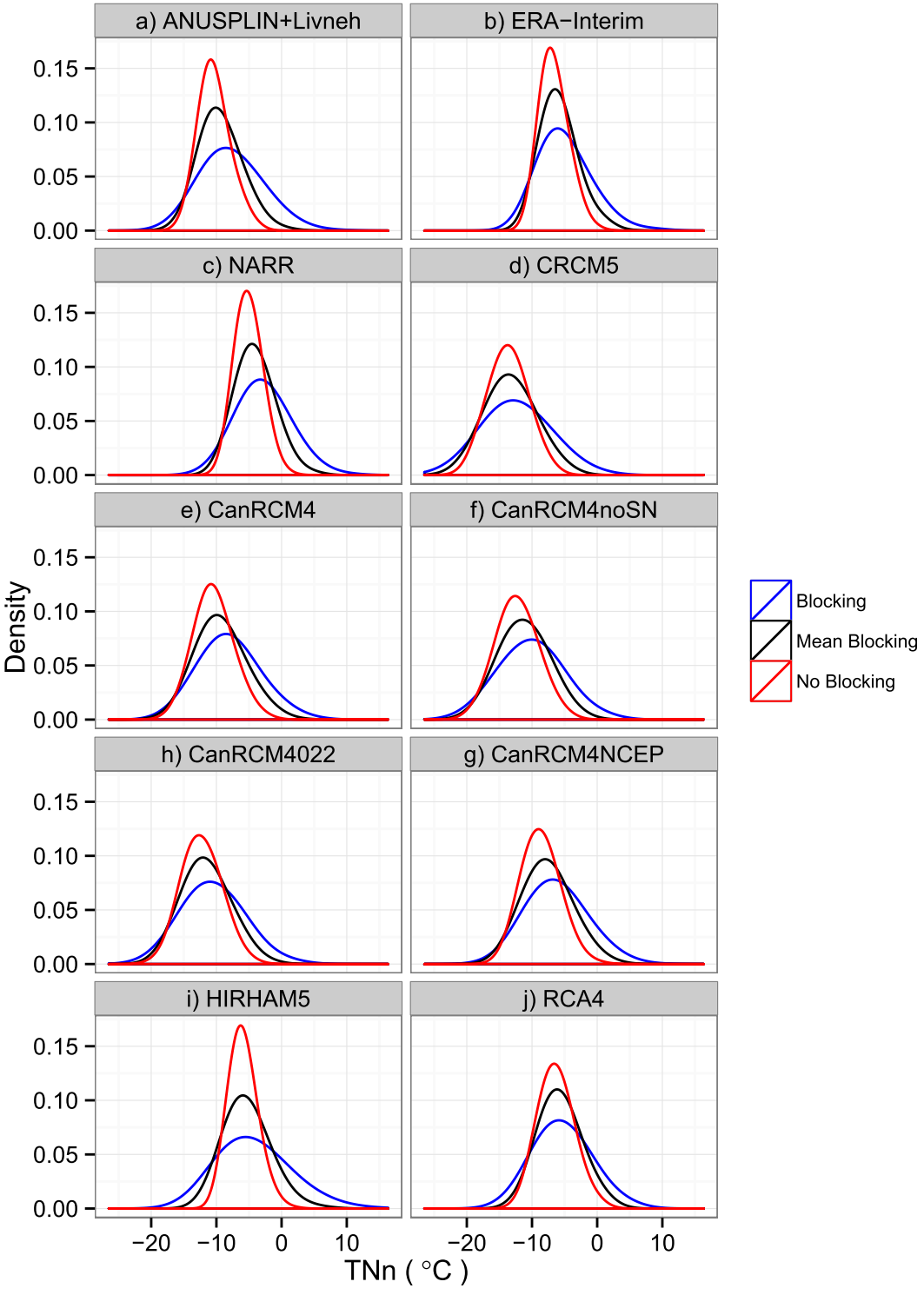

FIG. 9. As in Fig. 7, but for RegPP TNn.

We explored this relationship further in three regions where blocking has a consistent positive (RegPP), negative (RegNN), or mixed (RegNP) influence on the location and scale parameters. First, in RegNN (a region covering western and central Canada) increased BF is associated with a negative slope on both the location and log-transformed scale parameters, indicating a shift to cooler minimum temperatures with less variability under a high

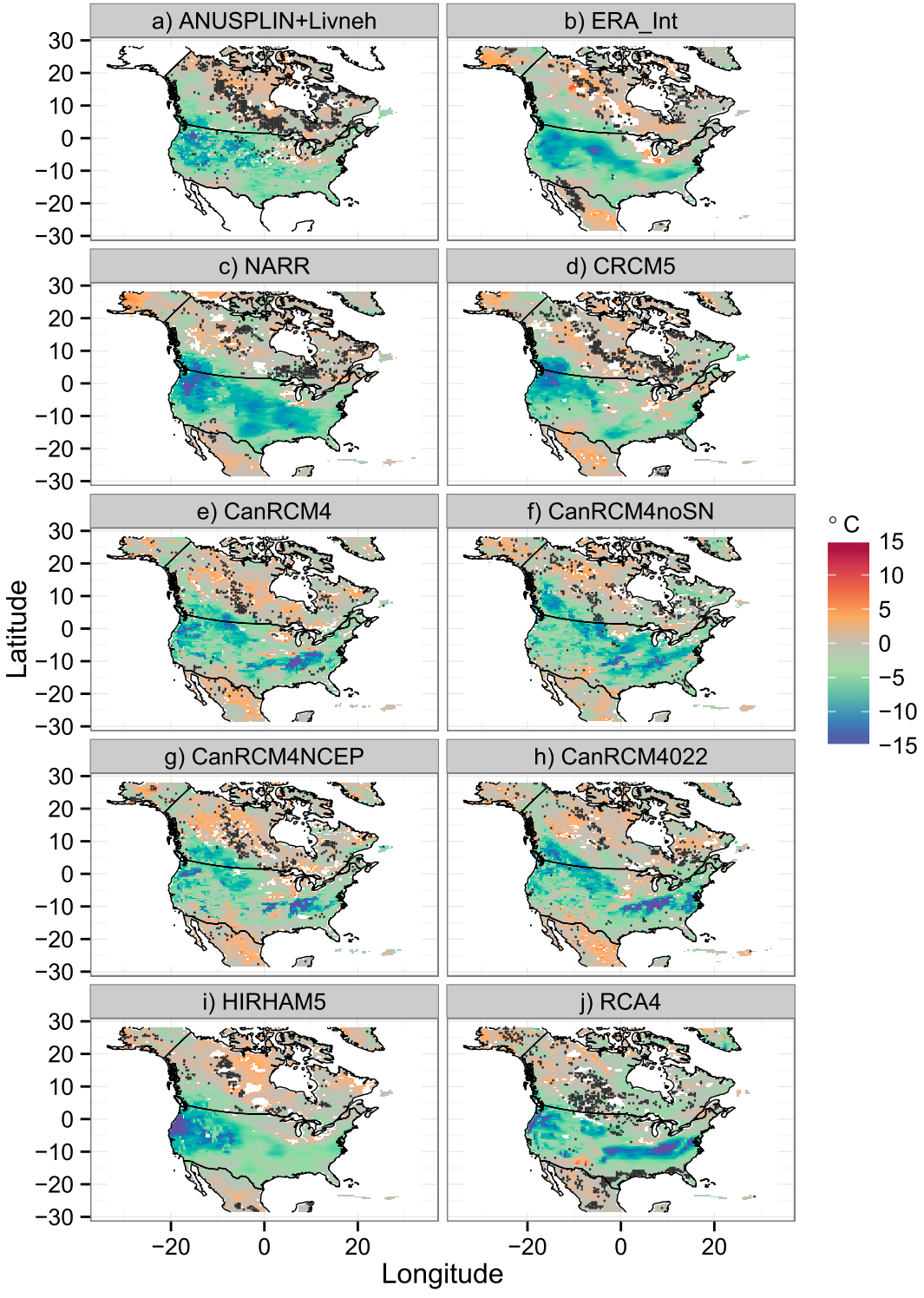

FIG. 10. The difference in the 20-yr return value of TNn (°C) when winter monthly BF is at the 90th and 10th percentiles in (a) ANUSPLIN+Livneh, (b) ERA-Interim, (c) NARR, (d) CRCM5, (e) CanRCM4, (f) CanRCM4noSN, (g) CanRCM4NCEP, (h) CanRCM4022, (i) HIRHAM5, and (j) RCA4. Pixels where the GEV is not a good fit for winter TNn are marked in gray.

blocking regime. In the eastern United States (RegNP) increased blocking is associated with a negative slope in the location parameter, but the influence on the scale parameter is mixed between datasets. In observations there is a positive slope on the log-transformed scale parameter, indicating that blocking is associated with cooler and more variable temperatures, while in NARR the slope is negative, indicating the blocking is associated with cooler and less variable extreme temperatures. Finally, in RegPP (the southwestern United States) increased BF is associated with a positive slope in both the location and log-transformed scale parameters, indicating warmer and more variable temperature extremes when BF is high. Changes in variability associated with atmospheric blocking can be relevant to predictability in a weather forecasting context, particularly in regions such as western Canada where variability of minimum temperature extremes decreases. An investigation of the extent to which these links are reproduced in weather forecasts at various lead times would provide a useful pathway for an aspect of process-based verification of minimum temperature predictions produced by weather forecast models.

The observed relationship between winter minimum temperatures and blocking is consistent with previous studies (Pfahl and Wernli 2012; Carrera et al. 2004; Favre and Gershunov 2006). Carrera et al. (2004) identified a similar region with an increased likelihood of cold mean and extreme temperatures under an Alaskan blocking regime. Their region extended southeast from the Yukon toward the southern plains of the United States and was characterized by cooler temperatures associated with reduced variance. The mechanisms of this relationship are reasonably well understood. Persistent anticyclones in the northeast Pacific advect cold air from polar regions into lower latitudes and promote clear skies (Pfahl and Wernli 2012; Favre and Gershunov 2006); evidence of this can be seen in the 500-hPa geopotential height anomalies in Fig. 1a and the vector wind anomalies in Fig. 2. Carrera et al. (2004) demonstrated that pronounced troughing occurs downstream over North America when the Alaskan region is blocked.

Furthermore, Carrera et al. (2004) identified a region in western Alaska where blocking is associated with warm temperatures (Carrera et al. 2004). This region was evident in the 20-yr return value difference in the reanalysis products over Alaska (ANUSPLIN+Livneh does not cover Alaska) and in all products over northwestern Canada. Previous work suggests there is little influence of warm air advection in collocated blocking events, instead attributing the warmer temperatures to adiabatic warming from subsidence and clear-sky radiative forcing (Pfahl and Wernli 2012).

In the southwestern United States (RegPP) blocking has a significant influence on both the location and scale parameters. This region of positive influence is not identified by previous studies as the increase in variability under a blocking regime results in overall lower extreme temperatures. Favre and Gershunov (2006) note the change of sign around the Mexican border in the correlation between cyclonic activity in the northeast Pacific and mean minimum temperature, which corresponds to the positive difference in return values.

The influence of blocking on the variability of TNn in RegNP is interesting as statistically significant impacts of opposite sign are detected in ANUSPLIN+Livneh and NARR. This region may be influenced by the strength of the South Atlantic high pressure cell. Carrera et al. (2004) found variability in the strength of this circulation within Alaskan blocking events, with stronger circulation associated with stronger southwesterly flow over the southeastern United States and increased precipitation in the Ohio River valley. Given the location of the Atlantic high toward the edge of the NARR domain, the reanalysis product may have some deficiencies in the simulation of this process. Variability in this region may also be related to the southerly penetration of cold fronts or modification of the intensity of cold air outbreaks related to differences in the snow line due to model temperature biases. Further work on this issue would be useful.

Regional climate model simulations are generally able to simulate the relationship between blocking and minimum temperature. Specifically, CRCM5 and HIRHAM5 reproduce the spatial pattern of blocking influence best. RCA4 and the CanRCM4 simulations do not capture the extension of significant blocking influence extending south into the United States.

Projections of blocking activity in the twenty-first century are mixed (Masato et al. 2013). An examination of future blocking activity showed that 4 out of 12 general circulation models (GCMs) show an increase in Pacific blocking activity under a high emissions scenario, while only 2 GCMs demonstrated a decrease in Pacific blocking (Masato et al. 2013). The nature of the relationship between projected atmospheric blocking and temperature in North America would be an interesting question for future work.

In general, RCMs running on a North American domain are able to realistically modulate the intensity of cold temperature extremes in response to North Pacific blocking in their driving data. Thus, they should be able to add value to high-resolution projections of changes in temperature extremes as they combine the appropriate modulation of extremes with the expected benefits of topographic forcing and the more detailed representation of the atmosphere and land–atmosphere coupling.

Acknowledgments. This work is supported by the Canadian Network for Regional Climate and Weather Processes (CNRCWP) and the Pacific Climate Impacts Consortium. CNRCWP is funded by the National Science and Engineering Research Council (NSERC). J. Sillmann is supported by the Research Council of Norway under the ClimateXL project (Grant 243953). ERA-Interim data used in this study were obtained from the ECMWF data server. We acknowledge the World Climate Research Programme's Working Group on Regional Climate and the Working Group on Coupled Modelling, the former coordinating body of CORDEX. We also thank the climate modeling groups (CCCma, UQAM, DMI, SMHI) for producing and making available their model output. We also acknowledge the Earth System Grid Federation infrastructure, an international effort led by the U.S. Department of Energy's Program for Climate Model Diagnosis and Intercomparison. We thank the anonymous reviewers for their comments.

REFERENCES

Abdella, K., and N. McFarlane, 1997: A new second-order turbulence closure scheme for the planetary boundary layer. *J. Atmos. Sci.*, **54**, 1850–1867, doi:10.1175/1520-0469(1997)054<1850:ANSOTC>2.0.CO;2.

Barker, H. W., J. N. S. Cole, J.-J. Morcrette, R. Pincus, P. Räisänen, K. von Salzen, and P. A. Vaillancourt, 2008: The Monte Carlo independent column approximation: An assessment using several global atmospheric models. *Quart. J. Roy. Meteor. Soc.*, **134**, 1463–1478, doi:10.1002/qj.303.

Barriopedro, D., R. García-Herrera, A. R. Lupo, and E. Hernández, 2006: A climatology of Northern Hemisphere blocking. *J. Climate*, **19**, 1042–1063, doi:10.1175/JCLI3678.1.

——, ——, and R. M. Trigo, 2010: Application of blocking diagnosis methods to general circulation models. Part I: A novel detection scheme. *Climate Dyn.*, **35**, 1373–1391, doi:10.1007/s00382-010-0767-5.

Benoit, R., J. Côté, and J. Mailhot, 1989: Inclusion of a TKE boundary layer parameterization in the Canadian regional finite-element model. *Mon. Wea. Rev.*, **117**, 1726–1750, doi:10.1175/1520-0493(1989)117<1726:IOATBL>2.0.CO;2.

Bonsal, B. R., X. Zhang, L. A. Vincent, and W. D. Hogg, 2001: Characteristics of daily and extreme temperatures over Canada. *J. Climate*, **14**, 1959–1976, doi:10.1175/1520-0442(2001)014<1959:CODAET>2.0.CO;2.

Carrera, M. L., R. W. Higgins, and V. E. Kousky, 2004: Downstream weather impacts associated with atmospheric blocking over the northeast Pacific. *J. Climate*, **17**, 4823–4839, doi:10.1175/JCLI-3237.1.

Casati, B., and R. de Elía, 2014: Temperature extremes from Canadian Regional Climate Model (CRCM) climate change projections. *Atmos.–Ocean*, **52**, 191–210, doi:10.1080/07055900.2014.886179.

Casola, J. H., and J. M. Wallace, 2007: Identifying weather regimes in the wintertime 500-hPa geopotential height field for the Pacific–North American sector using a limited-contour clustering technique. *J. Appl. Meteor. Climatol.*, **46**, 1619–1630, doi:10.1175/JAM2564.1.

Cheung, H. N., W. Zhou, H. Y. Mok, M. C. Wu, and Y. Shao, 2013: Revisiting the climatology of atmospheric blocking in the Northern Hemisphere. *Adv. Atmos. Sci.*, **30**, 397–410, doi:10.1007/s00376-012-2006-y.

Christensen, O. B., M. Drews, H. Christensen, K. Dethloff, K. Ketelsen, I. Hebestadt, and A. Rinke, 2006: The HIRHAM regional climate model version 5. Tech. Rep. 06-17, Danish Meteorological Institute, 22 pp.

Coles, S., 2001: *An Introduction to Statistical Modeling of Extreme Values*. Springer, 209 pp.

Cuxart, J., P. Bougeault, and J.-L. Redelsperger, 2000: A turbulence scheme allowing for mesoscale and large-eddy simulations. *Quart. J. Roy. Meteor. Soc.*, **126**, 1–30, doi:10.1002/qj.49712656202.

Dee, D. P., and Coauthors, 2011: The ERA-Interim reanalysis: Configuration and performance of the data assimilation system. *Quart. J. Roy. Meteor. Soc.*, **137**, 553–597, doi:10.1002/qj.828.

DeGaetano, A. T., 2009: Time-dependent changes in extreme-precipitation return-period amounts in the continental United States. *J. Appl. Meteor. Climatol.*, **48**, 2086–2099, doi:10.1175/2009JAMC2179.1.

Delage, Y., and C. Girard, 1992: Stability functions correct at the free convection limit and consistent for both the surface and Ekman layers. *Bound.-Layer Meteor.*, **58**, 19–31, doi:10.1007/BF00120749.

Diaconescu, E. P., P. Gachon, J. Scinocca, and R. Laprise, 2015: Evaluation of daily precipitation statistics and monsoon onset/retreat over western Sahel in multiple data sets. *Climate Dyn.*, **45**, 1325–1354, doi:10.1007/s00382-014-2383-2.

Diao, Y., J. Li, and D. Luo, 2006: A new blocking index and its application: Blocking action in the Northern Hemisphere. *J. Climate*, **19**, 4819–4839, doi:10.1175/JCLI3886.1.

Favre, A., and A. Gershunov, 2006: Extra-tropical cyclonic/anticyclonic activity in north-eastern Pacific and air temperature extremes in western North America. *Climate Dyn.*, **26**, 617–629, doi:10.1007/s00382-005-0101-9.

Fouquart, Y., and B. Bonnel, 1980: Computations of solar heating of the earth's atmosphere: A new parameterization. *Beitr. Phys. Atmos.*, **53**, 35–62.

Gilleland, E., 2014: extRemes: Extreme value analysis, version 2.0.7. R package. [Available online at https://cran.r-project.org/web/packages/extRemes/index.html.]

Giorgi, F., C. Jones, and G. Asrar, 2009: Addressing climate information needs at the regional level: The CORDEX framework. *WMO Bull.*, **58**, 175–183.

Grotjahn, R., and Coauthors, 2016: North American extreme temperature events and related large scale meteorological patterns: A review of statistical methods, dynamics, modeling, and trends. *Climate Dyn.*, **46**, 1151–1184, doi:10.1007/s00382-015-2638-6.

Kain, J. S., and J. M. Fritsch, 1990: A one-dimensional entraining/detraining plume model and its application in convective parameterization. *J. Atmos. Sci.*, **47**, 2784–2802, doi:10.1175/1520-0469(1990)047<2784:AODEPM>2.0.CO;2.

——, and ——, 1993: Convective parameterization for mesoscale models: The Kain-Fritsch scheme. *The Representation of Cumulus Convection in Numerical Models*, *Meteor. Monogr.*, Amer. Meteor. Soc., No. 46, 165–170.

Kalnay, E., and Coauthors, 1996: The NCEP/NCAR 40-Year Reanalysis Project. *Bull. Amer. Meteor. Soc.*, **77**, 437–471, doi:10.1175/1520-0477(1996)077,0437:TNYRP.2.0.CO;2.

Kanamitsu, M., W. Ebisuzaki, J. Woollen, S.-K. Yang, J. J. Hnilo, M. Fiorino, and G. L. Potter, 2002: NCEP–DOE AMIP-II Reanalysis (R-2). *Bull. Amer. Meteor. Soc.*, **83**, 1631–1643, doi:10.1175/BAMS-83-11-1631.

Keellings, D., and P. Waylen, 2015: Investigating teleconnection drivers of bivariate heat waves in Florida using extreme value analysis. *Climate Dyn.*, **44**, 3383–3391, doi:10.1007/s00382-014-2345-8.

Khairoutdinov, M., and Y. Kogan, 2000: A new cloud physics parameterization in a large-eddy simulation model of marine stratocumulus. *Mon. Wea. Rev.*, **128**, 229–243, doi:10.1175/1520-0493(2000)128<0229:ANCPPI>2.0.CO;2.

Kuo, H. L., 1965: On formation and intensification of tropical cyclones through latent heat release by cumulus convection. *J. Atmos. Sci.*, **22**, 40–63, doi:10.1175/1520-0469(1965)022<0040:OFAIOT>2.0.CO;2.

Li, J., and H. W. Barker, 2005: A radiation algorithm with correlated-*k* distribution. Part I: Local thermal equilibrium. *J. Atmos. Sci.*, **62**, 286–309, doi:10.1175/JAS-3396.1.

Li, L., W. Li, and J. Jin, 2015: Contribution of the North Atlantic subtropical high to regional climate model (RCM) skill in simulating southeastern United States summer precipitation. *Climate Dyn.*, **45**, 477–491, doi:10.1007/s00382-014-2352-9.

Livneh, B., E. A. Rosenberg, C. Lin, B. Nijssen, V. Mishra, K. M. Andreadis, E. P. Maurer, and D. P. Lettenmaier, 2013: A long-term hydrologically based dataset of land surface fluxes and states for the conterminous United States: Update and extensions. *J. Climate*, **26**, 9384–9392, doi:10.1175/JCLI-D-12-00508.1.

Lohmann, U., and E. Roeckner, 1996: Design and performance of a new cloud microphysics scheme developed for the ECHAM general circulation model. *Climate Dyn.*, **12**, 557–572, doi:10.1007/BF00207939.

Masato, G., B. J. Hoskins, and T. Woollings, 2013: Winter and summer Northern Hemisphere blocking in CMIP5 models. *J. Climate*, **26**, 7044–7059, doi:10.1175/JCLI-D-12-00466.1.

Max Planck Institute, 2013: CDO: Climate data operators. [Available online at https://code.zmaw.de/projects/cdo.]

McKenney, D. W., and Coauthors, 2011: Customized spatial climate models for North America. *Bull. Amer. Meteor. Soc.*, **92**, 1611–1622, doi:10.1175/2011BAMS3132.1.

Mesinger, F., and Coauthors, 2006: North American Regional Reanalysis. *Bull. Amer. Meteor. Soc.*, **87**, 343–360, doi:10.1175/BAMS-87-3-343.

Pfahl, S., and H. Wernli, 2012: Quantifying the relevance of atmospheric blocking for co-located temperature extremes in the Northern Hemisphere on (sub-)daily time scales. *Geophys. Res. Lett.*, **39**, L12807, doi:10.1029/2012GL052261.

Photiadou, C., M. R. Jones, D. Keellings, and C. F. Dewes, 2014: Modeling European hot spells using extreme value analysis. *Climate Res.*, **58**, 193–207, doi:10.3354/cr01191.

Rasch, P. J., and J. E. Kristjánsson, 1998: A comparison of the CCM3 model climate using diagnosed and predicted condensate parameterizations. *J. Climate*, **11**, 1587–1614, doi:10.1175/1520-0442(1998)011<1587:ACOTCM>2.0.CO;2.

R Development Core Team, 2014: The R project for statistical computing. [Available online at http://www.R-project.org/.]

Renwick, J., and J. Wallace, 1996: Relationships between North Pacific wintertime blocking, El Niño, and the PNA pattern. *Mon. Wea. Rev.*, **124**, 2071–2076, doi:10.1175/1520-0493(1996)124<2071:RBNPWB>2.0.CO;2.

Rex, D. F., 1950: Blocking action in the middle troposphere and its effect upon regional climate. *Tellus*, **2A**, 196–211, doi:10.1111/j.2153-3490.1950.tb00331.x.

Rotstayn, L. D., 1997: A physically based scheme for the treatment of stratiform clouds and precipitation in large-scale models. I: Description and evaluation of the microphysical processes. *Quart. J. Roy. Meteor. Soc.*, **123**, 1227–1282, doi:10.1002/qj.49712354106.

Samuelsson, P., and Coauthors, 2011: The Rossby Centre regional climate model RCA3: Model description and performance. *Tellus*, **63A**, 4–23, doi:10.1111/j.1600-0870.2010.00478.x.

Sass, B. H., L. Rontu, and P. Räisänen, 1994: HIRLAM-2 radiation scheme: Documentation and tests. Swedish Meteorological and Hydrological Institute HIRLAM Tech. Rep. 16, 42 pp. [Available online at http://hirlam.org/index.php/hirlam-documentation/doc_view/1307-hirlam-technical-report-no-16.]

Savijärvi, H., 1990: Fast radiation parameterization schemes for mesoscale and short-range forecast models. *J. Appl. Meteor.*, **29**, 437–447, doi:10.1175/1520-0450(1990)029<0437:FRPSFM>2.0.CO;2.

Scherrer, S. C., M. Croci-Maspoli, C. Schwierz, and C. Appenzeller, 2006: Two-dimensional indices of atmospheric blocking and their statistical relationship with winter climate patterns in the Euro-Atlantic region. *Int. J. Climatol.*, **26**, 233–249, doi:10.1002/joc.1250.

Scinocca, J., V. V. Kharin, Y. Jiao, M. Qian, M. Lazare, L. Solheim, and G. Flato, 2016: Coordinated global and regional climate modelling. *J. Climate*, **29**, 17–35, doi:10.1175/JCLI-D-15-0161.1.

Shabbar, A., J. Huang, and K. Higuchi, 2001: The relationship between the wintertime North Atlantic Oscillation and blocking episodes in the North Atlantic. *Int. J. Climatol.*, **21**, 355–369, doi:10.1002/joc.612.

Shepherd, T. G., 2014: Atmospheric circulation as a source of uncertainty in climate change projections. *Nat. Geosci.*, **7**, 703–708, doi:10.1038/ngeo2253.

Sillmann, J., M. Croci-Maspoli, M. Kallache, and R. W. Katz, 2011: Extreme cold winter temperatures in Europe under the influence of North Atlantic atmospheric blocking. *J. Climate*, **24**, 5899–5913, doi:10.1175/2011JCLI4075.1.

Sundqvist, H., E. Berge, and J. E. Kristjánsson, 1989: Condensation and cloud parameterization studies with a mesoscale numerical weather prediction model. *Mon. Wea. Rev.*, **117**, 1641–1657, doi:10.1175/1520-0493(1989)117<1641:CACPSW>2.0.CO;2.

Tibaldi, S., and F. Molteni, 1990: On the operational predictability of blocking. *Tellus*, **42A**, 343–365, doi:10.1034/j.1600-0870.1990.t01-2-00003.x.

Tiedtke, M., 1989: A comprehensive mass flux scheme for cumulus parameterization in large-scale models. *Mon. Wea. Rev.*, **117**, 1779–1800, doi:10.1175/1520-0493(1989)117<1779:ACMFSF>2.0.CO;2.

Tompkins, A. M., 2002: A prognostic parameterization for the subgrid-scale variability of water vapor and clouds in large-scale models and its use to diagnose cloud cover. *J. Atmos. Sci.*, **59**, 1917–1942, doi:10.1175/1520-0469(2002)059<1917:APPFTS>2.0.CO;2.

Tourpali, K., and P. Zanis, 2013: Winter anticyclonic blocking effects over Europe during 1960–2000 from an ensemble of regional climate models. *Climate Res.*, **57**, 81–91, doi:10.3354/cr01169.

Verseghy, D. L., 1991: CLASS—A Canadian land surface scheme for GCMS. I. Soil model. *Int. J. Climatol.*, **11**, 111–133, doi:10.1002/joc.3370110202.

von Salzen, K., N. A. McFarlane, and M. Lazare, 2005: The role of shallow convection in the water and energy cycles of the atmosphere. *Climate Dyn.*, **25**, 671–688, doi:10.1007/s00382-005-0051-2.

Wang, X., Y. Feng, and L. A. Vincent, 2013: Observed changes in one-in-20 year extremes of Canadian surface air

temperatures. *Atmos.–Ocean*, **52**, 222–231, doi:10.1080/07055900.2013.818526.

Whan, K., and F. W. Zwiers, 2016a: Evaluation of extreme rainfall and temperature over North America in CanRCM4 and CRCM5. *Climate Dyn.*, **46**, 3821–3843, doi:10.1007/s00382-015-2807-7.

——, and ——, 2016b: The impact of ENSO and the NAO on extreme winter precipitation in North America in observations and regional climate models. *Climate Dyn.*, doi:10.1007/s00382-016-3148-x, in press.

——, J. Zscheischler, R. Orth, M. Shongwe, M. Rahimi, E. Asare, and S. I. Seneviratne, 2015: Impact of soil moisture on extreme maximum temperatures in Europe. *Wea. Climate Extremes*, **9**, 57–67, doi:10.1016/j.wace.2015.05.001.

Zadra, A., D. Caya, J. Cote, B. Dugas, C. Jones, R. Laprise, K. Winger, and L. Caron, 2008: The next Canadian Regional Climate Model. *Phys. Can.*, **64**, 75–83.

Zhang, G., and N. A. McFarlane, 1995: Sensitivity of climate simulations to the parameterization of cumulus convection in the Canadian Climate Centre general circulation model. *Atmos.–Ocean*, **33**, 407–446, doi:10.1080/07055900.1995.9649539.

Zhang, X., J. Wang, F. W. Zwiers, and P. Y. Groisman, 2010: The influence of large-scale climate variability on winter maximum daily precipitation over North America. *J. Climate*, **23**, 2902–2915, doi:10.1175/2010JCLI3249.1.